Int. J. Electrochem. Sci., 10 **(2015)** 8158 - 8174

International Journal of
ELECTROCHEMICAL
SCIENCE
www.electrochemsci.org

In Vitro Degradation and Cytotoxicity Evaluation of Iron Biomaterials with Hydroxyapatite Film

Renáta Oriňaková[1,*], *Andrej Oriňak*[1], *Miriam Kupková*[2], *Monika Hrubovčáková*[2], *Lucia Markušová-Bučková*[1], *Mária Giretová*[2], *Ľubomír Medvecký*[2], *Edmund Dobročka*[3], *Ondrej Petruš*[1], *František Kaľavský*[1]

[1] Department of Physical Chemistry, Faculty of Science, P.J. Šafárik University, Moyzesova 11, SK-04154 Košice, Slovak Republic
[2] Institute of Materials Research, Slovak Academy of Science, Watsonova 47, SK-04353 Košice, Slovak Republic
[3] Institute of Electrical Engineering, Slovak Academy of Sciences, Dúbravská cesta 9 SK-841 04 Bratislava, Slovak Republic
[*]E-mail: Renata.Orinakova@upjs.sk

Received: 9 June 2015 / *Accepted:* 12 August 2015 / *Published:* 26 August 2015

Biodegradable metallic materials have attracted considerable interest due to their use for temporary medical implants. Coating of metallic implants by bioactive materials like hydroxyapatite (HAp) ceramics is widely used to improve the osteointegration and to ensure the lasting clinical success. The biodegradable iron material was produced by sintering of carbonyl iron powder and coated with electrochemically deposited hydroxyapatite and manganese-doped HAp (MnHAp) ceramics layer. Formation of HAp was proved by XRD analysis. The electrochemical and static immersion corrosion behaviour of developed materials in Hank's solution was studied. The degradation rate after 13 weeks of immersion as well as the corrosion rate determined from polarisation curves was in the sequence: Fe + HAp, Fe + MnHAp, Fe, from lower to higher. The moderate negative effect of bioceramic coating on the in vitro cytotoxicity was observed.

Keywords: carbonyl iron, powder metallurgy, hydroxyapatite, electrodeposition, corrosion behaviour, cytotoxicity

1. INTRODUCTION

In recent years, biomaterials have been extensively studied for their obvious use as replacements of various body parts or even organs [1]. The main goal of tissue engineering is the functional *in vivo* reconstruction of damaged tissue, and *in vitro* regeneration of tissue architecture [2, 3]. The choice of biomaterials is the most important issue for the achievement of tissue engineering

practice [4, 5]. It is desirable for the biomaterials used in the tissue repairing to have advantageous mechanical properties and biocompatible surfaces [4]. Poor biocompatibility may cause adverse biological reactions, such as inflammation, and thrombus formation [6, 7]. The bioactive materials should have the ability to promote production and organization of extracellular matrix, direct attachment, proliferation and differentiation of cells [4, 8-10]. Biodegradable materials have attracted considerable interest due to their use for temporary medical implants in osteosynthesis and cardiovascular applications [9, 11–19]. In orthopedic applications, these materials should retain required mechanical strength over critical phases of the tissue repairing to allow a gradual load transfer to the healing bone as the materials degrade [9, 17]. The biodegradable implants should be osteoconductive, and should circumvent long-term clinical issues [9,15, 17, 20, 21]. They also save the second surgery to remove the implant which is common with non-degradable metallic implants [9, 14, 15, 22].

Magnesium- and iron-based alloys are two suitable classes of biodegradable implant material [9, 11, 15, 22-30]. One approach to improve the osteointegration and to ensure the lasting clinical success of metallic implants is by coating bioactive materials like hydroxyapatite ($Ca_{10}(PO_4)_6(OH)_2$ named shortly HAp) ceramics on such constructs [1, 4, 30-35]. HAp is the essential mineral element (69 wt.%) of human hard tissues. HAp with Ca/P ratio within the range 1.50 - 1.67 is known to enhance bone repairing [4, 9, 32, 34, 36]. In their synthetic form, these bioactive ceramics form direct bonds with adjacent hard tissues via dissolution and ion exchange with body fluids [34]. It exhibited very good biocompatibility with bones, skin and muscles, teeth, both *in vitro* and *in vivo* [4]. HAp belongs to very effective bioceramics in the clinical healing of hard-tissue injury and illness with bioactivity that supports cell proliferation, bone ingrowth, osseointegration, and harden in situ [4, 9, 31, 37]. HAp has been widely used in many areas of medicine, such as orthopedics and dentistry, but mainly for contact with bone tissue, due to its close similarity of chemical composition and high biocompatibility with natural bone tissue [4, 9, 35, 38, 39]. This bioactive ceramic material is also degradable with different solubility in body environment [9].

Manganese-doped HAp (MnHAp) with good corrosion resistance and *in vitro* bioactivity has been reported by several researchers [31, 40-44]. The introduction of Mn^{2+} into HAp coating resulted in considerable reduction of porosity, enhancement of ligand binding affinity of integrins, activation of cellular adhesion, and improvement its interaction with the host bone tissue [31, 41, 42, 45]. The significant improvement of the quality and rate of bone repair was achieved due to this composite material in biocoating technology [31, 40].

Various coating methods are being used for the deposition of HAp coatings onto implant surfaces such as plasma spray, dip coating, sol-gel, electrochemical deposition, electrophoretic, radio frequency sputtering, magnetron sputtering, micro-arc oxidation, and pulsed laser [1, 32, 34, 35, 46-50]. Plasma spray has been widely used for the fabrication of HAp [32, 35, 48]. However, this method has several disadvantages, such as non-uniformity in the coating density, poor adhesion between the substrate and coating layer, formation of microcracks, phase changes owing to high temperature application, and improper microstructural control, which could lead to failure of the implanted device [1, 32, 35].

Electrochemical deposition is more appropriate due to the availability and low cost, the low temperatures involved, the ability to coat porous surfaces and substrates of complex shape, the possibility to regulate the uniformity, microstructure, composition, and thickness of the deposit by adjusting current or voltage, and the potential enhancement of the coating/substrate bond strength [1, 31, 32, 34, 35, 51, 52].

The degradation rate of the degradable biomaterials for orthopaedic applications should correspond to the rate of bone tissue remodelation in order to allow a fluent load transmission from the scaffold to the bone. In our previous studies, the iron based sintered materials were evaluated as a potential degradable biomaterial [53, 54]. The developed materials have showed a quite low *in vitro* biodegradation rate and high cytotoxicity. For this reason, the thin incoherent bioceramic coating layer was suggested to improve the biocopmatibility but not decrease the degradation rate of the iron based sintered materials. The effect of Mn^{2+} ion concentration in plating bath and deposition time period on the composition, quantity, quality, surface morphology, and corrosion stability of developed samples was investigated in our previous work [55]. No significant influence of thin bioceramic coating layer on the degradation behaviour of sintered iron material was registered. The aim of present study was the more detailed investigation of *in vitro* degradation behaviour and cytotoxicity evaluation. Electrochemical corrosion tests were extended and complemented with static immersion corrosion tests. Biocompatibility was evaluated by fluorescent staining and *in vitro* cytotoxicity testing.

2. EXPERIMENTAL PART

2.1 Preparation of materials

The iron samples were prepared from carbonyl iron powder (CIP) fy BASF (type CC, d50 value 3.8 – 5.3 μm) with composition: 99.5 % Fe, 0.05 % C, 0.01 % N and 0.18 % O by cold pressing into pellets (Ø 10 mm, h 2 mm) at 600 MPa followed by sintering in a tube furnace at 1120°C in reductive atmosphere (10 % H_2 and 90 % N_2) for 1 hour.

2.2 Electrochemical deposition of HAp and MnHAp coatings

Prior to electrodeposition of bioceramic layer the surface of sintered Fe pellets was finished gradually with SiC papers of different grits (240, 800 and 1500). Thereafter, the substrate material was ultrasonically cleaned in acetone, anhydrous ethanol and washed with distilled water.

Electrochemical deposition of bioceramic coating layer was realized using an Autolab PGSTAT 302N potentiostat. Polished and cleaned Fe pellet was used as the working electrode, Ag/AgCl/KCl (3 mol/l) as reference electrode, and Pt sheet as counter electrode. The electrolyte solution used for electrodeposition of HAp layer was composed of 2.5 x 10^{-2} mol/l $NH_4H_2PO_4$ (analytical grade), 4.2 x 10^{-2} mol/l $Ca(NO_3)_2$ (analytical grade). Electrolyte for deposition of MnHAp layer contained besides the mentioned compounds also 3.0 x 10^{-3} mol/l $Mn(NO_3)_2$ (analytical grade). Cathodic deposition was performed under the following parameters: pH 4.3 ± 0.5, 0.85 mA/cm^2 current density, 40 min and 65 ± 0.5 °C. Subsequently, the coated iron pellets were treated as follows:

soaking in 1 mol/l NaOH solution at 65 °C for approximately 2 h, washing in distilled water and drying at 80 °C for 2 h. Finally, the coated samples were sintered for 2 h at 400 °C in N_2.

2.3 Characterization of materials

The surface morphology of prepared samples was assessed by scanning electron microscope coupled with the energy dispersive spectrometer (JEOL JSM-7000F, Japan with EDX INCA).

XRD analysis was performed using Bruker D8 DISCOVER diffractometer equipped with X-ray tube with rotating Cu anode operating at 12 kW (40kV/300 mA). The measurements were carried out in parallel beam geometry with parabolic Goebel mirror in the primary beam. The X-ray fluorescence background was suppressed by LiF monochromator inserted in the diffracted beam. The X-ray diffraction patterns were recorded in grazing incidence set-up with the angle of incidence $\alpha = 12°$ in the angular range 20 - 80°.

The content of Mn in MnHAp coating was determined by atomic absorption spectrometry (AAS) PERKIN-ELMER 420 after dissolution in nitric acid.

The morphology, distribution, and density of the cells were evaluated using an inverted optical microscope Leica DM IL LED.

The absorbance of formazan was determined by an UV VIS spectrophotometer UV -1800, Shimadzu at 490 nm.

2.4 Electrochemical degradation test

The electrochemical corrosion tests were carried out on the uncoated and bioceramic coated samples included open circuit potential (OCP) time measurements and potentiodynamic polarisation measurements. The corrosion behaviour was evaluated in Hank's solution contained 8 g/l NaCl, 0.4 g/l KCl, 0.14 g/l $CaCl_2$, 0.06 g/l $MgSO_4.7H_2O$, 0.06 g/l $NaH_2PO_4.2H_2O$, 0.35 g/l $NaHCO_3$, 1.00 g/l Glucose, 0.60 g/l KH_2PO_4 and 0.10 g/l $MgCl_2.6H_2O$ in double distilled water at pH 7.4. All degradation studies were performed at 37±2°C. The electrochemical measurements were carried out by means of an Autolab PGSTAT 302N potentiostat in three-electrode system with the uncoated or bioceramic coated Fe sample as the working electrode, Ag/AgCl/KCl (3 mol/l) as reference electrode, and Pt sheet as counter electrode. For OCP- time measurements, the samples were immersed in Hank's solution and the OCP was monitored under equilibrated conditions for an hour. The potentiodynamic polarisation curves were registered after stabilization of the free corrosion potential from -800 mV to -200 mV (vs. Ag/AgCl/KCl (3 mol/l)) at a scanning rate of 0.1 mV/s.

2.5 Static immersion test

The immersion test was performed also in Hank's solution with a pH value of 7.4. Experimental samples were immersed in 10 ml solutions and the temperature was kept at 37 °C using a heating mantle. After weighting for initial weights (m_i), samples were subjected to the ultrasonic cleaning in acetone and ethanol for 10 min each. The corroded samples were removed from

the solution after every 7 days of immersion, ultrasonically cleaned in distilled water and ethanol for 10 min each, air dried and weighed. The corrosion rate was determined from the weight loss as follows:

$$CR = \frac{m_i - m_f}{At} \quad (1)$$

where, *CR* stands for the corrosion rate, m_f is the final mass after corrosion, *A* represents the surface area exposed to the Hank's solution and *t* is the immersion time [56].

2.6 Cytotoxicity test

2.6.1 Fluorescent staining

MC3T3E1 cells in subconfluency were harvested from culture flasks by enzymatic digestion (trypsin-EDTA solution). The cells were suspended in culture medium and the cell suspension was adjusted to density of 7.5 x 10^4 cells/ml. The samples in the form of tablets, stainless steel and titanium sheets (control) were sterilized at 170 °C for 1 hour in thermostat after cleaning in ethanol. Samples were placed on the bottom of wells of the 48- well microplate (not cell culture treated), 3 x 10^4 of MC3T3E1 cells in the 400 µl of Dulbecco´s modified Eagle´s medium (DMEM) with 10 % FBS and 1 % ATB-antimycotic solution (Sigma-Aldrich) were seeded to each well. The culture plate was cultivated in incubator at 37 ºC, 95 % humidity and 5 % CO_2. After 4 hours of cultivation, the density, distribution and morphology of the cells were evaluated on the tested samples using a fluorescence optical microscopy and live/dead staining based on fluorescein diacetate (FDA)/propidium iodide (PI). FDA is upon hydrolysis by intracellular esterases of living cells converted to green fluorescent product contrary to the PI that passes only the damaged membranes of dead cells and stains the cells red.

2.6.2 In vitro cytotoxicity testing of substrates

MC3T3E1 cells in subconfluency were harvested from culture flasks by enzymatic digestion (trypsin-EDTA solution) and suspended in culture medium. 2 x 10^4 of MC3T3E1 cells in the 400 µl of Dulbecco´s modified Eagle´s medium (DMEM) with 10 % fetal bovine serum (FBS) and 1 % ATB-antimycotic solution (Sigma-Aldrich) were seeded to each well of the 48- well microplate and cultured in incubator at 37 ºC, 95 % humidity and 5 % CO_2 for 24 hours. After cultivation, the silicone rings (thickness 1mm) were placed on bottom of wells. Samples in the form of tablets and stainless steel sheet (control) were placed on the top of rings after sterilization at 170 °C for 1 hour in thermostat. The cytotoxicity testing was carried out according to STN ISO 10993-5:2009. The culture plate was cultivated in incubator at 37 ºC, 95 % humidity and 5 % CO_2 for 24 hours. The wells with cells were twice washed with phosphate saline buffer after removing substrates and silicone rings from wells. The cytotoxicity of samples was evaluated by a commercially purchased proliferation test (the Cell titer 96 aqueous one solution cell proliferation assay, Promega, USA) according to the manufacturer´s instructions. The absorbance of the final product (formazan) was determined at 490 nm.

3. RESULTS AND DISCUSSION

Mass of bioceramic coating deposited onto the surface of sintered iron samples determined from the mass difference after and before the coating layer deposition was about 3.6 mg and 2.4 mg for HAp and MnHAp coating layer, respectively. Content of Mn in MnHAp coating layer was about 0.5 wt.%. Deposited coating layers were adhesive and stable.

3.1 SEM analysis of bioceramic coating layer

Surface morphologies of sintered Fe sample and Fe materials coated with HAp and MnHAp layers are presented in Fig.1. It can be seen that the surface of uncoated Fe sample was relatively smooth and dense. SEM analysis of the coated Fe samples revealed the incoherent irregular bioceramic coating layers obtained by electrodeposition. Star-like HAp microstructures with different dimensions formed by triangular thin plates (with length about 5 – 10 μm, width below 1 μm and thickness 100 – 300 nm) were observed for HAp coating layer. The addition of Mn in coating layer resulted in completely different surface morphology. The individual circular-shaped structures with diameter about 10 μm and oval-shaped assemblies formed by several circular blocks were observed for MnHAp coating layer. The cracked nodular surface appearance with unevenly distributed rod-like nanostructures could be seen at higher magnification.

The presence of HAp components in both coating layers was proved by EDX analysis. Average compositions of the surface of coated iron samples at different positions are referred in Table 1 and Table 2 for HAp and MnHAp layer, respectively. Average compositions were calculated form 10 – 15 elemental EDX point analyses performed on several samples. Results proved the presence of HAp largely in position 1 and partially in position 3 while the presence of iron oxides predominantly in positions 3 and 2. The Ca/P ratio in HAp coating layer was between 1.39 and 1.78. The mole ratio of Ca to P of stoichiometric HAp is 1.67.

EDX analysis of the surface of MnHAp coated sample revealed the highest content of HAp in position 5 together with low amount of iron oxides. Small amount of HAp was detected also in position 4 together with Mn and iron oxides. Content of iron in position 4 was two times higher than in position 5. Position 6 corresponded to the uncoated iron substrate. The content of Mn obtained by point analysis was about 3.21 wt.%. It appeared together with Fe in larger needle aggregates with low HAp content on the surface of coating layer. The Ca/P molar ratio in MnHAp coating layer was between 1.37 and 1.61.

These results indicate that biocearmic layers prepared were slightly Ca-deficient. The Ca/P ratio in HAp and MnHAp coating layers electrochemically deposited on NaOH-treated Ti substrate by Huang et al. [31] was 1.1 and 1.13, respectively. In contrast, Ca/P ratios in HAp layers electrodeposited by Jamesh et al. [57] on pure magnesium substrate and by Su et al. [58] on magnesium alloy substrate were 1.666 and 1.667, respectively.

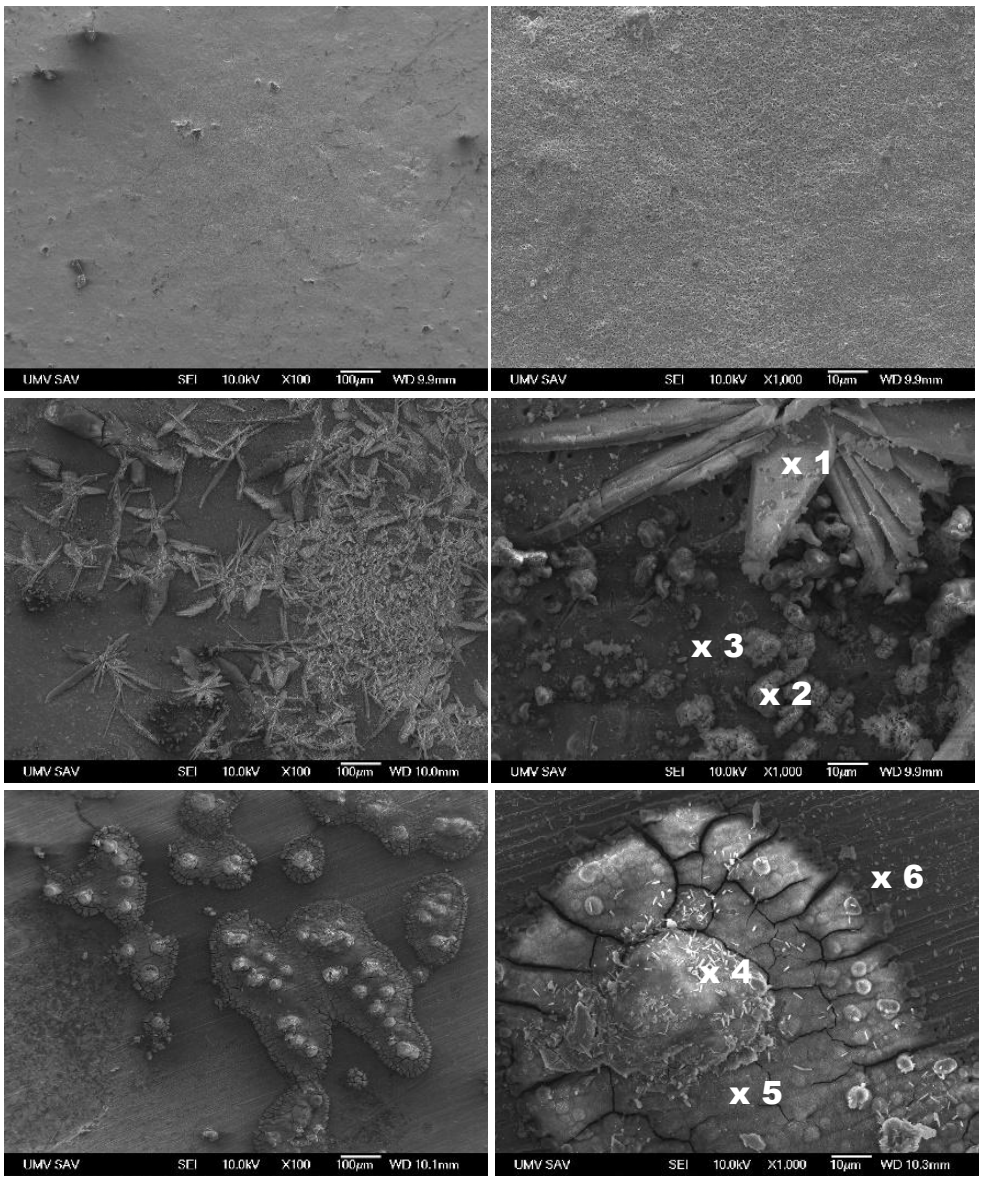

Figure 1. SEM micrographs of the surface of uncoated and bioceramic coated Fe material: Fe (a, b); Fe + HAp (c, d); Fe + MnHAp (e. f).

Table 1. Chemical composition of the surface of powder-metallurgical iron samples coated with HAp layer at different positions marked in Fig. 1d.

Element	Average composition					
	Position 1		Position 2		Position 3	
	wt.%	at.%	wt.%	at.%	wt.%	at.%
C K	3.74	7.45	1.26	3.47	1.93	6.16
O K	34.8	52.1	24.8	51.4	13.4	32.6
Na K	2.20	2.29	0.75	1.09	0.59	0.86
P K	18.8	14.5	0.56	0.60	2.79	3.46
Ca K	37.2	22.2	1.05	0.87	3.94	3.77
Fe K	3.31	1.42	71.6	42.6	77.4	53.1

Table 2. Chemical composition of the surface of powder-metallurgical iron samples coated with MnHAp layer at different positions marked in Fig. 1f.

Element	Average composition					
	Position 4		Position 5		Position 6	
	wt.%	at.%	wt.%	at.%	wt.%	at.%
C K	3.92	9.95	2.69	6.44	0.48	1.99
O K	24.2	46.2	22.2	39.9	3.30	10.4
Na K	2.05	2.73	4.11	5.15	0.26	0.58
P K	3.49	3.44	14.7	13.7	0.49	0.80
Ca K	6.40	4.88	28.6	20.6	0.71	0.89
Fe K	56.7	31.00	27.7	14.3	94.8	85.4
Mn K	3.21	1.78	-	-	-	-

3.2 XRD analysis of bioceramic coating layer

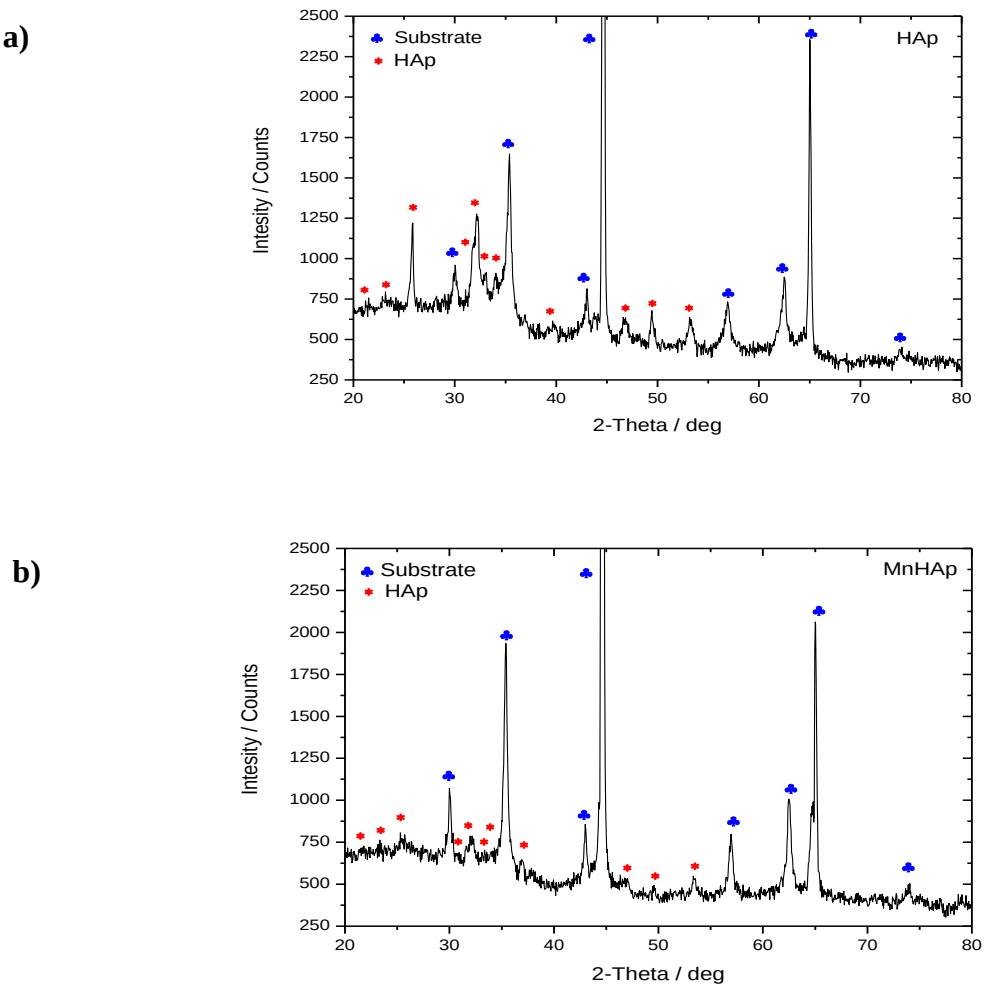

Figure 2. XRD patterns of HAp and MnHAp coatings on the surface of Fe substrate.

The XRD patterns of the HAp (Fig. 2a) and MnHAp (Fig. 2b) coatings are given in Fig. 2. Typical peaks of HAp were identified in both patterns. For the MnHAp coating (Fig. 2b), the typical main peaks of the lattice planes (21–31) at 2θ = 31.77° and (11-22) at 32.20° were reduced in comparison to HAp coating. This behaviour could be associated with the creation of a new phase containing Mn compounds. Several rather broad reflections are still observed in the X-ray diffraction profile which could be ascribed to the presence of nanocrystalline HAp phase resulting from the interference of the HAP crystal structure formation with the dopant compounds. From the XRD pattern of the HAp and MnHAp layers, it could be concluded that grown HAp favours hexagonal phase and consists of two phases, an ordered phase and a nanocrystalline phase.

3.3 Electrochemical corrosion behaviour

The OCP–time plots for the uncoated and bioceramic coated Fe materials at 37 °C are shown in Fig.3. The OCP of coated materials was found to be shifted to less negative potential compared to the uncoated sample, showing higher thermodynamic stability. The values of initial potential were about -500 mV, -420 mV and -370 mV for uncoated Fe sample, MnHAp coated and HAp coated sample, respectively. The continual decrease in potential was observed for bioceramic coated samples. The slight decrease followed by slight increase in potential and its saturation at certain value was registered for uncoated Fe substrate. The OCP in Hanks' solution reached a potential of about -500 mV, -495 mV and -440 mV (vs. Ag/AgCl/KCl (3 mol/l)) after 60 minutes for uncoated Fe sample, MnHAp coated and HAp coated sample, respectively. This indicated that the incoherent bioceramic coating layer did not deteriorate significantly the biodegradation behaviour of material.

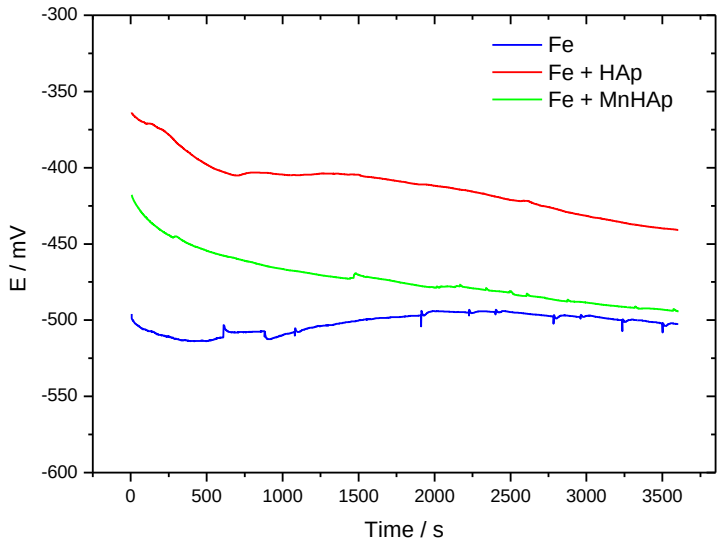

Figure 3. OCP–time measurements of sintered Fe material without and with bioceramic coating layer obtained in Hank's solution at constant time of 60 min.

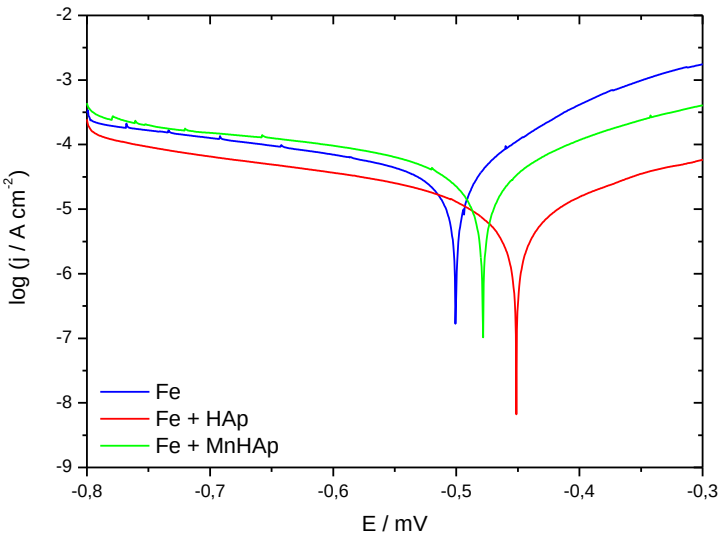

Figure 4. Potentiodynamic polarisation curves of sintered Fe material without and with bioceramic coating layer obtained in Hank's solution at pH 7.4 and 37°C at scan rate 0.1 mV/s.

Degradation behaviour of developed material in Hank's solution was studied by anodic polarisation curves. Fig. 4 shows characteristic potentiodynamic polarisation curves for the uncovered Fe sample and Fe samples coated with HAp and MnHAp layers in Hank's solution at 37 °C. The values of corrosion current density (j_{corr}), corrosion potential (E_{corr}), anodic and cathodic Tafel slopes (b_a, b_c) and average corrosion rates derived from polarisation curves are listed in Table 3.

Table 3. Calculated values of E_{corr}, j_{corr}, b_a, b_c and corrosion rates of sintered Fe material without and with bioceramic coating layer obtained from the potentiodynamic polarisation curves in Hank's solution at pH 7.4 and 37°C.

vzorka	E_{corr} (mV)	j_{corr} (μA/cm^2)	Corrosion rate (mm/year)	b_a (mV/dec)	b_c (mV/dec)
Fe	-500.6	41.88	0.4853	467.1	82.19
Fe + HAp	-452.0	13.62	0.1578	263.9	189.5
Fe + MnHAp	-478.3	23.84	0.2762	318.8	180.4

All the curves showed similar corrosion behaviour. The values of E_{corr} shifted to the less negative potential side for both bioceramic coated samples indicating the increased corrosion resistance of coated samples as compared to bare Fe sample. The highest corrosion susceptibility was observed for MnHAp coated sample. Corrosion potential of uncoated Fe was about -500 mV, while E_{corr} of the HAp coated and MnHAp coated iron substrate was about -452 mV and -478 mV. The increased corrosion resistance of coated materials was proved also by decreasing values of j_{corr} and corrosion rate. The value of *in vitro* degradation rate in Hank's solution for the sample with MnHAp coating layer was nearly two times higher than that of the HAp coated Fe sample, which could be associated with presence of Mn in coating layer. Cathodic Tafel slope refer to hydrogen ion reduction,

and its value is generally about 120 mV. Anodic Tafel lines correspond to the corrosion process of examined samples and are associated with dissolution of iron. Decrease in b_c values for bioceramic coated samples as compared to uncoated iron sample gave another indication of corrosion inhibition due to HAp and MnHAp coating layers. This result shows that the incoherent bioceramic coatings layer served as a slight barrier layer against corrosion. The shift of E_{corr} values to the positive potential side as well as the decrease in j_{corr} values due to coating of Ti samples with HAp and MnHAp layer was observed also by Huang et al. [31]. Decrease in corrosion rate of magnesium alloy WE43 due to the hydroxyapatite reinforcement was reported also by Dieringa et al. [59]. Corrosion protective ability of HAp coating layer with the thickness 2-3 μm was proved also by Jamesh et al. [57]. Ulum et al. [9] have observed shift of corrosion potential of composite Fe-HAp material in Kokubo's solution to more negative potential as compared to pure Fe material, while the corrosion rate of Fe material was higher than that of composite material Fe-HAp.

3.4 Static immersion corrosion behaviour

The mass losses of the samples during static immersion test in Hank's solution for 13 weeks are shown in Fig. 5. The highest weight loss during the first two week of immersion was obtained for MnHAp coated iron material, which can be associated with presence of Mn in the coating layer. The highest mass loss during next two week was nearly the same for all the samples. The highest mass loss was registered for uncoated iron material, while the lowest one for HAp coated sample during remaining weeks of immersion. The continual increase in difference between the mass losses for individual samples was detected. The weight changes together with mass loss after every week for three examined samples are listed in Table 4.

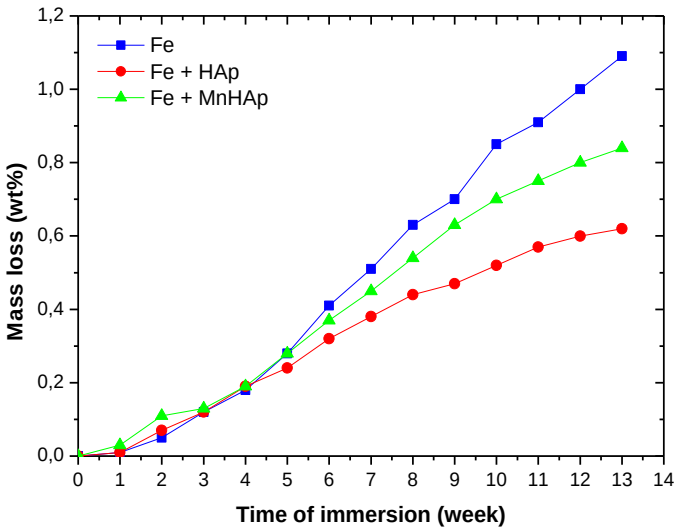

Figure 5. The mass loss during immersion in Hank's solution for 13 weeks for uncoated and bioceramic coated iron materials.

A comparison of corrosion rates calculated from mass losses after 2, 4, 6, 8, 10 and 13 weeks of immersion test in Hank's solution shows Table 5. The highest corrosion rate after two weeks of immersion was proved for bioceramic coating layer with pre presence of Mn. However, also the corrosion rate for HAp coated sample was higher than that of uncoated material. The HAp presence in both coating layers enhanced the surface hydrophilicity and was thus considered to decrease the corrosion resistance of bioceramic coated samples [2]. The slight increase in corrosion rates of coated samples and rather higher increase in corrosion rate of uncoated sample occurred during longer immersion period.

Table 4. Values of mass loss after every week of immersion in Hank's solution for uncoated and bioceramic coated iron materials together with the actual mass of samples.

week	Mass (mg)			Mass loss (mg)			Mass loss (wt %)		
	Fe	Fe + HAp	Fe + MnHAp	Fe	Fe + HAp	Fe + MnHAp	Fe	Fe + HAp	Fe + MnHAp
0	909.20	916.42	915.17	0	0	0	0	0	0
1	909.11	916.29	914.86	0.09	0.13	0.31	0.01	0.01	0.03
2	908.78	915.77	914.19	0.42	0.65	0.98	0.05	0.07	0.11
3	908.10	915.33	913.95	1.10	1.09	1.22	0.12	0.12	0.13
4	907.60	914.71	913.43	1.60	1.71	1.74	0.18	0.19	0.19
5	906.66	914.20	912.57	2.54	2.22	2.60	0.28	0.24	0.28
6	905.48	913.53	911.76	3.72	2.89	3.41	0.41	0.32	0.37
7	904.55	912.92	911.08	4.65	3.50	4.09	0.51	0.38	0.45
8	903.43	912.38	910.27	5.77	4.04	4.90	0.63	0.44	0.54
9	902.81	912.07	909.39	6.39	4.35	5.78	0.70	0.47	0.63
10	901.48	911.64	908.74	7.72	4.78	6.43	0.85	0.52	0.70
11	900.89	911.22	908.33	8.31	5.20	6.84	0.91	0.57	0.75
12	900.10	910.89	907.88	9.10	5.53	7.29	1.00	0.60	0.80
13	899.27	910.70	907.49	9.93	5.72	7.68	1.09	0.62	0.84

Table 5. Values of corrosion rate determined from mass loss after immersion in Hank's solution for uncoated and bioceramic coated iron materials after 2, 4, 6, 8, 10 and 13 weeks of immersion.

week	Corrosion rate (mg/m^2 day)		
	Fe	Fe +HAp	Fe + MnHAp
2	0.951	1.471	2.218
4	1.811	1.935	1.969
6	2.807	2.180	2.573
8	3.265	2.286	2.773
10	3.495	2.164	2.911
13	3.458	1.992	2.674

The corrosion rates as high as 3.458 mg/m^2 day, 1.992 mg/m^2 day, and 2.674 mg/m^2 day were obtained after 13 weeks for uncoated, HAp coated and MnHAp coated sample, respectively. It can be seen that the corrosion rate after two weeks of immersion increased as the following: Fe, Fe + HAp, Fe + MnHAp, while after 6 and more weeks was degradation rate in the sequence: Fe + HAp, Fe + MnHAp, Fe, from lower to higher. The same trend was observed for corrosion rates determined from polarisation curves.

From the results of degradation studies it can be concluded that the presence of Mn in the bioceramic coating increased corrosion rate and decreased corrosion resistance of MnHAp coated iron material, particularly in the first stages of degradation.

3.5 Determination of in-vitro cytotoxicity

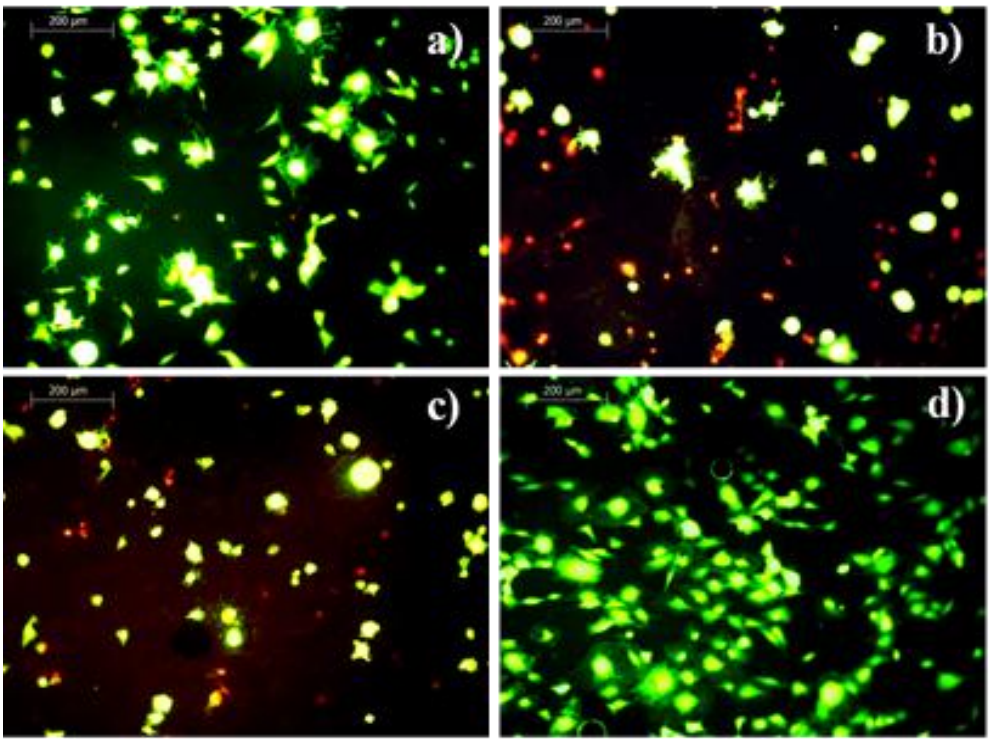

Figure 6. Fluorescent optical micrographs of osteoblasts on surface of metallic samples after 4 hour adherence (live/dead staining): a) Fe; b) Fe+HAp; c) Fe-MnHAp; d) Ti.

Fluorescent optical micrographs presented in Fig. 6 show the morphology and distribution of osteoblasts on the surface of metallic substrates after 4 hour adherence in culture medium at 37 °C. A denser osteoblast layer was visible on the uncoated Fe substrate in comparison with bioceramic coated samples on which the higher amount of dead cells (red color) was observed. Besides the cell morphologies on Fe sample were closer to these ones found on titanium surface. Osteoblasts on titanium sheet were perfectly spreaded with visible filopodia corresponding to non cytotoxic character of surface.

The relative viabilities of MC3T3E1 cells cultivated for 24 hours in relation to the negative control (stainless steel sheet) are shown in Fig. 7. The relative viability was determined from values of relative absorbance of the formazan produced by cells during enzyme catalysis via the mitochondrial dehydrogenase in wells after removing of samples and stainless steel sheet. The reason for above experimental arrangement was the reduction of contact effect of partially oxidized sample surface on proliferation of cells and the cytotoxicity of sample extracts was practically measured. Despite of the cytotoxicity of extracts could be affected by the production of hydrated iron oxides during the cultivation, which was verified by the fine turbidity of DMEM after culture.

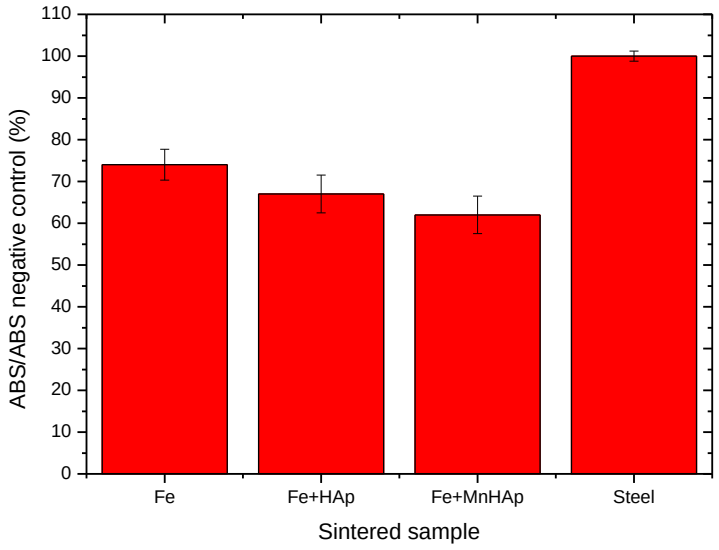

Figure 7. Relative viability of MC3T3E1 cells expressed as the ratio of formazan absorbance in wells with sample to absorbance of formazan in wells with stainless steel.

From ANOVA analysis resulted that absorbance of uncoated Fe sample and control were statistically different ($p < 0.008$). Similarly formazan absorbance of MnHAp coated sample differs from absorbance of uncoated Fe sample ($p < 0.102$) contrary to absorbance of samples with HAp and MnHAp coating layer, which were not statistically different ($p > 0.05$). The proliferation activity of cells in wells after cultivation with uncoated Fe substrate achieved about 80% of proliferation activity of osteoblasts in wells after cultivation with stainless steel substrate whereas formazan production of cells affected by culture with MnHAp or HAp coated substrates decreased to around 60% absorbance

of control sample. From comparison resulted a low cytotoxicity of extracts from Fe material while bioceramic coated samples could be potentially cytotoxic.

From these results it can be concluded that the thickness of hydroxyapatite coating was probably insufficient for improving of bioactivity or minimization of the *in vitro* cytotoxicity of samples. Because of above facts and the porosity of hydroxyapatite layer, the culture medium can strongly affect the surface of samples with the formation of hydrated Fe oxides, which were gradually exfoliated from samples simultaneously with hydroxyapatite particles and cells were not able to adhere and proliferate on such unstable surfaces.

These results are in agreement with findings of Ito et al. [2]. They deposited HAp particles on poly(3-hydroxybutyrate-co-3-hydroxyvalerate) nanofibrous film. It was concluded by the authors that the cell adhesion was not significantly affected by presence of HAp.

4. CONCLUSIONS

In this study, the electrochemical deposition of thin and incoherent HAp and MnHAp layer has been carried out onto the sintered iron substrate surface with the aim to improve their biocompatibility but not deteriorate their degradation rate. Formation of nanocrystalline HAp ceramic layer was proved by XRD analysis. EDX analysis revealed the Ca/P molar ratio in bioceramic coating between 1.37 and 1.78. The degradation rate determined from both electrochemical corrosion test and immersion corrosion test increased as the following: Fe + HAp, Fe + MnHAp, Fe. The thickness of hydroxyapatite coating was insufficient for minimization of the *in vitro* cytotoxicity of samples.

ACKNOWLEDGEMENTS
The authors wish to acknowledge financial support from the Slovak Research and Development Agency, Projects APVV-0677-11 and APVV-0280-11, Grant Agency of the Ministry of Education of the Slovak Republic, Grant No. 1/0211/12.

References

1. B. Ghiban, G. Jicmon and G. Cosmeleata, *Rom. Journ. Phys.* 51 (2006) 187
2. Y. Ito, H. Hasuda, M. Kamitakahara, C. Ohtsuki, M. Tanihara, I.-K. Kang, O.H. Kwon, *J. Biosci, Bioeng.* 100 (2005) 42
3. R. Langer, J.P. Vacanti, *Science* 260 (1993) 920
4. A. Costan, N. Forna, A. Dima, M. Andronache, C. Roman, V. Manole, L. Stratulat, M. Agop, *J. Optoelectron. Adv. Mater.* 13 (2011) 1338
5. N. Cimpoeşu, S. Stanciu, M. Meyer, I. Ioniţă, R. Hanu Cimpoeşu, *J. Optoelectron. Adv. Mater.* 12 (2010) 386
6. Y. Jiang, Y. Liang, H. Zhang, W. Zhang, S.Tu, *Mater. Sci. Eng.* C 41 (2014) 1
7. D. Kwak, Y. Wu, T.A. Horbett, *J. Biomed. Mater. Res.* 74A (2005) 69
8. C.H. Chang, F.H. Lin, T.F. Kuo, H.C. Liu, *Biomed. Eng.- App. Bas. C.* 17 (2005) 1
9. M.F. Ulum, A. Arafat, D. Noviana, A.H. Yusop, A.K. Nasution, M.R. Abdul Kadir, H. Hermawan, *Mater. Sci. Eng. C* 36 (2014) 336

10. A.H. Yusop, A.A. Bakir, N.A. Shaharom,M.R. Abdul Kadir, H. Hermawan, *Int. J. Biomater.* 2012 (2012) Article ID 641430
11. B. Heublein, R. Rohde, V. Kaese, M. Niemeyer,W. Hartung, A. Haverich, *Heart* 89 (2003) 651
12. A.G.A. Coombes, M.C. Meikle, *Clin. Mater.* 17 (1994) 35
13. M. Peuster, P. Wohlsein, M. Bru¨gmann, M. Ehlerding, K. Seidler, C. Fink, H. Brauer, A. Fischer and G. Hausdorf, *Heart* 86 (2001) 563
14. M. Peuster, C. Hesse, T. Schloo, C. Fink, P. Beerbaum, C. von Schnakenburg, *Biomaterials* 27 (2006) 4955
15. M. Schinhammer, I. Gerber, A.C. Hänzi and P.J. Uggowitzer, *Mater. Sci. Eng. C* 33 (2013) 782
16. M. Moravej, D. Mantovani, *Int. J. Mol. Sci.* 12 (2011) 4250
17. S.C. Rizzi, D.J. Heath, A.G.A. Coombes, N. Bock, M. Textor and S. Downes, *J. Biomed. Mater. Res.* 55 (2001) 475
18. P. Erne, M. Schier, T.J. Resink, *Cardiovasc. Intervent. Radiol.* 29 (2006) 11
19. F. Witte, N. Hort, C. Vogt, S. Cohen, K.U. Kainer, R. Willumeit, F. Feyerabend, *Curr. Opin. Solid State Mater. Sci.* 12 (2009) 63
20. B.S. Lee, J.K. Lee, W.J. Kim, Y.H. Jung, S.J. Sim, J. Lee, I.S. Choi, *Biomacromolecules* 8 (2007) 744
21. A.E. Özçam, K.E. Roskov, J. Genzer , R.J. Spontak, *Appl. Mater. Interfaces*4 (2012) 59
22. F. Witte, V. Kaese, H. Haferkamp, E. Switzer, A. Lindenberg-Meyer, C.J. Wirth, H. Windhagen, *Biomaterials* 26 (2005) 3557.
23. M. Schinhammer, A.C. Hänzi, J.F. Löffler, P.J. Uggowitzer, *Acta Biomater.* 6 (2010) 1705
24. R. Waksman, R. Pakala, R. Baffour, R. Seabron, D. Hellinga, F.O. Tio, *J. Interv. Cardiol.* 21 (2008) 15
25. B. Liu, Y.F. Zheng, *Acta Biomater.* 7 (2011) 1407
26. H. Hermawan, H. Alamdari, D. Mantovani, D. Dube, *PowderMetall.* 51 (2008) 38
27. E. Zhang, H. Chen, F. Shen, *J. Mater. Sci. Mater. Med.* 21 (2010) 2151
28. H. Hermawan, D. Dube, D. Mantovani, *J. Biomed. Mater. Res. A* 93 (2010) 1
29. F. Witte, J. Fischer, J. Nellesen, H.A. Crostack, V. Kaese, A. Pisch, F. Beckmann, H. Windhagen, *Biomaterials* 27 (2006) 1013
30. F. Witte, F. Feyerabend, P. Maier, J. Fischer, M. Störmer, C. Blawert, W. Dietzel, N. Hort, *Biomaterials* 28 (2007) 2163
31. Y. Huang, Q. Ding, S. Han, Y. Ya, X. Pang, *J. Mater. Sci. Mater. Med.* 24 (2013) 1853
32. N. Norziehana CheIsa, Y. Mohd, N. Yury, Electrodeposition of Hydroxyapatite (HAp) Coatings on Etched Titanium Mesh Substrate, 2012 IEEE Colloquium on Humanities, Science & Engineering Research (CHUSER 2012), December 3-4, 2012, Kota Kinabalu, Sabah, Malaysia, p.771 - 775
33. C. Delabarde, C.J.G. Plummer, P.-E.Bourban, J.-A.E. Manson, *J. Mater. Sci. Mater. Med.* 23 (2012) 1371
34. N. Eliaz, M. Eliyahu, *J. Biomed. Mater. Res.* 80A (2007) 621
35. A. Kar, K.S. Raja, M. Misra, *Surf. Coat. Technol.* 201 (2006) 3723–3731
36. K.Y. Renkema, R.T. Alexander, R.J. Bindels, J.G. Hoenderop, *Ann. Med.* 40 (2008) 82
37. J.H. Shepherd, D.V. Shepherd, S.M. Best, *J. Mater. Sci. Mater. Med.* 23 (2012) 2335
38. K.S. Raja, M. Misra, K. Paramguru, *Mater.Lett.* 59 (2005) 2137
39. C. Ohtsuki, M. Kamitakahara, T. Miyazaki, *J. R. Soc. Interface.* 6 (2009) S349
40. I. Mayer, F.J.G. Cuisinier, S. Gdalya, I. Popov, *J. Inorg. Biochem.* 102 (2008) 311
41. B. Bracci, P. Torricelli, S. Panzavolta, E. Boanini, R. Giardino, A. Bigi, *J. Inorg. Biochem.* 103 (2009) 1666
42. Y. Li, J. Widodo, S. Lim, C.P. Ooi, *J. Mater. Sci.* 47 (2012) 754
43. E. Gyorgy, P. Toricelli, G. Socol, M. Iliescu, I. Mayer, I.N. Mihailescu, A. Big , J. Werckman, *J. Biomed. Mater. Res.* 71A (2004) 353

44. A. Bigi, B. Bracci, F. Cuisinier, R. Elkaim, M. Fini, I. Mayer, I.N. Mihailescu, G. Socol, L. Sturba, P. Torricelli, *Biomaterials*26 (2005) 2381
45. I. Sopyan, S. Ramesh, N.A. Nawawi, A. Tampieri, S. Sprio, *Ceram. Int.* 27 (2011) 3703
46. S. Robler, A. Sewing, M. Slolzer, R. Born, D. Schanweber, M. .Dard, H. Worch, *J. Biomed. Mater. Res.* 64A (2002) 655.
47. M. S. Kim, J. J. Ryu, Y. M. Sung, *Electrochem. Comm.* 9 (2007) 1886
48. P. Peng, S. Kumar, N. H. Voelcker, E. Szili, R. C. Smart, H. J. Griesser, *J. Biomed. Mater. Res.* 76A (2005) 347
49. V. Nelea, C. Ristoscu, C. Chiritescu, C. Ghica, I. N. Mihailescu, H. Peletier, P. Mille, A. Cornet, *Appl. Surf. Sci.* 168 (2000) 127
50. D. Y. Lin, X. X. Wang, *Surf. Coat. Technol.* 204 (2010) 3205
51. X. Yang, B. Zhang, J. Lu, J. Chen, X. Zhang, Z. Gu, *Appl. Surf. Sci.* 256 (2010) 2700
52. M.S. Djosic, V. Panic, J. Stojanovic, M. Mitric, V.B. Miskovic-Stankovic, *Colloid. Surf.* A. 400 (2012 36
53. A. Oriňak, R. Oriňaková, Z. Orságová Králová, A. Morovská Turoňová, M. Kupková, M. Hrubovčáková, J. Radoňák, R. Džunda, *J. Porous Mater.* 21 (2014) 131
54. R. Oriňaková, A. Oriňak, L. Markušová Bučková, M. Giretová, Ľ. Medvecký, E. Labbanczová, M. Kupková, M. Hrubovčáková, K. Kovaľ, *Int. J. Electrochem. Sci.* 8 (2013) 12451
55. R. Oriňaková, A. Oriňak, M. Kupková, M. Hrubovčáková, L. Škantárová, A. Morovská Turoňová, L. Markušová Bučková, C. Muhmann, H.F. Arlinghaus, *Int. J. Electrochem. Sci.* 10 (2015) 659
56. B. Wegener, B. Sievers, S. Utzschneider, P. Müller, V. Jansson, S. Rößler, B. Nies, G. Stephani, B. Kieback, P. Quadbeck, *Mater. Sci. Eng. B.* 176 (2011) 1789
57. M. Jamesh, Satendra Kumar, T.S.N. Sankara Narayanan, J. Coat. Technol. Res. 9 (2012) 495
58. Y. Su, G. Li, J. Lian, *Int. J. Electrochem. Sci.* 7 (2012) 11497
59. H. Dieringa, L.Fuskova, D. Fechner, C. Blawert, Proceedings of ICCM17 Edinburgh, 27-31 July 2009, Edinburgh, UK (B1:9)

© 2015 The Authors. Published by ESG (www.electrochemsci.org). This article is an open access article distributed under the terms and conditions of the Creative Commons Attribution license (http://creativecommons.org/licenses/by/4.0/).